IOPscience iopscience.iop.org

Home Search Collections Journals About Contact us My IOPscience

Photoreflectance investigations of the energy level structure in GaInNAs-based quantum wells

This article has been downloaded from IOPscience. Please scroll down to see the full text article.

2004 J. Phys.: Condens. Matter 16 S3071

(http://iopscience.iop.org/0953-8984/16/31/006)

View the table of contents for this issue, or go to the journal homepage for more

Download details:
IP Address: 129.252.86.83
The article was downloaded on 27/05/2010 at 16:21

Please note that terms and conditions apply.

INSTITUTE OF PHYSICS PUBLISHING JOURNAL OF PHYSICS: CONDENSED MATTER

J. Phys.: Condens. Matter **16** (2004) S3071–S3094 PII: S0953-8984(04)74824-9

Photoreflectance investigations of the energy level structure in GaInNAs-based quantum wells

J Misiewicz[1], **R Kudrawiec**[1], **K Ryczko**[1], **G Sęk**[1], **A Forchel**[2], **J C Harmand**[3] **and M Hammar**[4]

[1] Institute of Physics, Wrocław University of Technology, Wybrzeże Wyspiańskiego 27, 50-370 Wrocław, Poland
[2] Institute of Physics, Würzburg University, Am Hubland, D-97074, Würzburg, Germany
[3] Laboratoire de Photonique et de Nanostructures, CNRS Route de Nozay 91460 Marcoussis, France
[4] Department of Microelectronics and Information Technology, Royal Institute of Technology (KTH), Electrum 229, S-16440 Kista, Sweden

E-mail: jan.misiewicz@pwr.wroc.pl

Received 12 January 2004
Published 23 July 2004
Online at stacks.iop.org/JPhysCM/16/S3071
doi:10.1088/0953-8984/16/31/006

Abstract
In this paper, we present the application of photoreflectance (PR) spectroscopy to investigate the energy level structure of GaInNAs-based quantum wells (QWs). Series of single GaInNAs/GaAs QWs with different nitrogen and indium contents are analysed. The electron effective mass (m_e^*) and conduction band offset (Q_C) are determined and compared with the literature data. The Q_C in GaInNAs/GaAs system in the range of investigated GaInNAs content (28–41% of In, 0.3–5.3% of N) has been found to be almost the same as for GaInAs/GaAs system, i.e. $Q_C \approx 0.8$. In addition, the energy level structure for the step-like GaInNAs/Ga(In)NAs/GaAs QWs tailored at 1.3 and 1.55 μm and the Sb-containing Ga(In)NAs/GaAs QWs is investigated. Also, the character of PR transitions, the influence of rapid thermal annealing (RTA) on the energy level structure, and the influence of the carrier localization effect on the efficiency of PR photomodulation are discussed.

1. Introduction

Semiconductor lasers operating at 1.3 and 1.55 μm wavelengths are very important light sources for fibre telecommunication. For these wavelengths there are windows of zero dispersion and minimized damping in the currently installed fibres. Up to now lasers at these wavelengths have been almost exclusively fabricated from GaInAsP or AlGaInAs heterostructures on InP. Recently, a novel GaAs-based material system (i.e. GaInNAs/GaAs

© 2004 IOP Publishing Ltd Printed in the UK

QW) has been proposed for this application [1]. GaAs-based lasers offer a number of advantages, as compared to InP-based structures, including higher temperature insensitivity of the laser threshold and output, which could allow for uncooled operation of the devices. Also, in the case of GaAs-based structures it is easy to grow a good GaAs/AlAs distributed Bragg reflectors (DBR) structure for vertical-cavity surface-emitting lasers (VCSEL). Moreover, the use of GaInNAs as an alternative material system offers cost-effective production on large-scale-GaAs substrates [2, 3].

The role of nitrogen atoms in III–V compounds (i.e. GaAs, GaInAs) is two-fold: nitrogen atoms cause the bulk bandgap to decrease dramatically, and the smaller lattice constant of GaN results in lower strain in GaInNAs, as compared to GaInAs. However, with an increasing nitrogen mole fraction, the optical quality of the material usually deteriorates significantly, resulting in a higher threshold current density of lasers. In order to improve the performance of 1.3 and 1.55 μm GaInNAs/GaAs QW lasers, the nitrogen composition of the GaInNAs well should be considerably small, commonly no more than 1%, although this will lead to an increased strain for getting the corresponding wavelength. Nowadays, the GaInNAs/GaAs lasers present very competitive characteristics at 1.3 μm wavelength [2, 4–6], but it remains difficult to obtain this good performance at longer emission wavelengths. Optimal values which are typically used for 1.3 emission are, respectively, 35% In and 1% N. Higher indium composition increases the compressive strain to a critical point for the structural quality of the QW. Higher nitrogen composition introduces non-radiative centres, which results in poor optical properties. For these reasons, other approaches were developed to redshift the emission wavelength and to keep good optical quality [7]. One of them is to introduce strain-compensated layers to this GaInNAs/GaAs QW structure [8–13], thus the active region of such a laser structure is a step-like QW. The other approach is to incorporate Sb atoms into GaInNAs compounds [14–16]. In addition, the nitrogen-containing structures are very often annealed because this significantly enhances PL intensity, although it simultaneously shifts the bandgap energy to blue [17–19]. All mentioned modifications influence the energy structure of GaInNAs/GaAs QWs. In this paper we focus on the investigation of the energy level structure in GaInNAs-based systems and its evolution due to the introduction of step-like barriers, Sb atoms and RTA. In order to investigate the energy level structure we have applied PR spectroscopy [20, 21].

PR spectroscopy utilizes the modulation of the built-in electric field at the semiconductor surface or interface through photo-injection of electron–hole pairs generated by a chopped incident laser beam. It is equivalent to a non-contact form of electroreflectance. This technique produces sharp spectral features related to the critical points of the band structure even at room temperature. It is a very important aspect of material characterization since devices normally operate around room temperature. Unlike other techniques such as photoluminescence (PL), which show only ground state QW transitions, PR yields energies of barrier and higher-order QW transitions. This provides a more strict comparison with the theoretical models and can give reliable information about such factors as the band offset or the electron effective mass. Moreover, PR spectroscopy which is an absorption-type method is not sensitive to defect states, and the combination of a PR experiment with an emission-type experiment, e.g. PL, becomes a very powerful tool to investigate optical processes in semiconductor structures. In addition, PR is contactless and therefore non-destructive, which is useful for characterization during various stages of device fabrication. So far, many important bulk parameters such as bandgap energies, alloy compositions, doping concentrations, built-in electric fields, and surface Fermi energies have been determined by using PR spectroscopy. Since the end of 1980s PR spectroscopy has become one of the fundamental tools to investigate the energy levels in QW structures [20, 21].

2. Experiment

Both molecular beam epitaxy (MBE) and metal-organic vapour-phase epitaxy (MOVPE) grown samples were used in this study. All samples were grown on unintentionally doped (100) GaAs substrates. MBE samples were grown at Wurzburg University (WU) in Germany and at the Laboratoire de Photonique et de Nanostructures (LPN) CNRS in France. MOVPE samples were grown at the Royal Institute of Technology (KTH) in Sweden. More details about MOVPE and MBE machines and growth processes can be found elsewhere [9, 22, 23]. To determine the nitrogen and indium contents, both high resolution x-ray diffraction and pre-calibrated PL investigations of the samples were preformed. The PR experiments were performed using a tungsten halogen lamp as a probe light source. For photomodulation, the 635 nm line of a semiconductor laser was employed as a pump beam. A single grating 0.55 m monochromator and a thermoelectrically cooled GaInAs *pin* photodiode were used to analyse the reflected light. The details of the PR apparatus are described elsewhere [21].

3. Results

3.1. The energy level structure of GaInNAs/GaAs QWs: electron effective mass and band offset determination

Most practical optoelectronic devices adopt QW structures. Hence, the knowledge of the bandgap energy, the number of confined electron and hole states, the electron effective mass and the band offset is necessary. In this section we present the PR approach to investigate these issues. Also, a review of these subjects and some conclusions are presented in this section.

3.1.1. Theoretical approach. The most striking features in the Ga(In)NAs system are the dramatic reduction in fundamental bandgap energy and the huge increase in electron effective mass. Shan *et al* [24] have shown that these unusual behaviours can be quite well understood within a simple band anticrossing (BAC) model. In this model the incorporation of nitrogen atoms into a host matrix compound (GaAs or GaInAs) leads to a strong interaction between the conduction band and a narrow resonant band formed by the nitrogen states. The interaction between the extended conduction states of the matrix semiconductor and the localized nitrogen states is treated as a perturbation which leads to the following eigenvalue problem:

$$\begin{vmatrix} E - E_M & V_{MN} \\ V_{MN} & E - E_N \end{vmatrix} \tag{1}$$

where E_M are the conduction states of the matrix semiconductor, E_N are the localized states, related to nitrogen atoms, and V_{MN} is the matrix element describing the interaction between E_M and E_N. Solving the eigenvalue problem gives the following subband energies:

$$E_{\pm} = \tfrac{1}{2}\left[E_N + E_M \pm \sqrt{[E_N - E_M]^2 + 4V_{MN}^2}\right]. \tag{2}$$

V_{MN} and E_N have to be extracted experimentally, and many authors have investigated these parameters so far [24–28]. Lindsay and O'Reilly [29] have found that for nitrogen-diluted GaAs the V_{MN} element varies with the nitrogen content as $V_{MN} = C_{MN}\sqrt{x}$, where C_{MN} is the coupling constant and x is the nitrogen content. They have also obtained that E_M and E_N vary with the nitrogen content according to $E_N = E_N^0 - \gamma x$ and $E_M = E_0 - \alpha x$, respectively, where $E_N^0 = 1.675$ eV, $\gamma = 2.52$ eV, $\alpha = 1.55$ eV, and E_0 is the energy of the Ga(In)NAs compound in the absence of nitrogen atoms.

Klar *et al* [30] have shown by using the tight-binding supercell calculation method that the bandgap energy of GaInNAs changes dramatically with the change in the nitrogen nearest-neighbour environment from four Ga to four In atoms. Duboz *et al* [31] have adapted results obtained by Klar to the BAC model by the modification of E_N parameter. The influence of RTA on the BAC parameters has been investigated in [28].

It should be underlined that numerous investigations of the BAC parameters were focused either on the GaNAs ternary compound or on GaInNAs layers lattice matched to GaAs, even though some of the most promising results for laser diodes have been obtained using highly strained, high In content GaInNAs QWs (see for example [2, 4]). For such a system the material parameters are usually extrapolated from the low In content GaInNAs compounds because bulk-like GaInNAs layers with a high In content cannot be grown on GaAs substrate due to the strain limit. Hence, some controversies associated with the value of the bandgap energy can appear for GaInNAs compounds with a high In content.

Calculations in the framework of an empirical pseudopotential method have shown that the band structure of Ga(In)NAs compounds is more complicated [32]. The structure includes two types of electronic states. First, there are the nitrogen pairs or other atomic cluster states that are created randomly in the bulk during growth. The localized energy levels due to nitrogen related clusters are formed around the conduction band either in the gap or in the continuum. Second, the perturbed host states represent mixing of the Γ–X–L and other conduction states by the N-induced perturbation. Hence, we rather should have a coupling and anticrossing of Γ, X, and L edges instead of the two-level BAC approach where only the interaction of the conduction band with the localized nitrogen level is taken into account. Therefore, using the BAC model actually means that we replace the complex interaction with higher-energy states by the coupling to only one 'effective' nitrogen level to get a simple empirical description of the Ga(In)NAs band structure. In general, the 'effective' nitrogen level may not correspond to a real state. However, in order to find the bandgap energy of the GaInNAs compound the BAC model is quite sufficient. The biggest advantage of the BAC model is its simplicity and quite good agreement with experimental data, hence we confine our theoretical approach to the BAC model.

The calculations of QW energy levels were performed within the framework of the usual envelope function approximation [33]. The excitonic effect was neglected. In order to find the bandgap energy of GaInNAs compound, we have adopted the BAC model with typical parameters: $E_N = 1.65$ eV, $E_M = E_g$ (GaInAs), and $C_{NM} = 2.7$ eV. We do not vary these parameters with the increase in nitrogen and indium contents. According to the BAC model, the influence of nitrogen-localized states on the valence band structure is neglected. Hence, we have assumed that the effective mass of light- and heavy-hole does not change after adding nitrogen atoms. In our calculations, we have included strain effects. The biaxial strain was calculated based on the Pikus–Bir Hamiltonian [34] as in [35]. The energy shifts due to hydrostatic δE_H and shear δE_S strain components equal

$$\delta E_H = 2a\left(1 - \frac{C_{12}}{C_{11}}\right)\varepsilon, \tag{3}$$

$$\delta E_S = 2b\left(1 - 2\frac{C_{12}}{C_{11}}\right)\varepsilon, \tag{4}$$

where ε is the strain tensor in the plane of the interfaces, C_{11} and C_{12} are elastic stiffness constants, and a and b are the hydrostatic and shear deformation potentials, respectively. All the parameters have been obtained by linear interpolation between the parameters of a relevant binary semiconductor [36]. In our calculations, we have considered m_e^* and Q_C as fitting parameters. In order to find the optimal value for m_e^* and Q_C parameters we have several times

repeated the following procedure. In the first step we determine the electron effective mass, i.e. we fit the calculated energy of the ground state transition to experimental data at fixed Q_C (the same as for GaInAs/GaAs QW) and free m_e^* parameter. The conduction band offset is determined in the next step. In this step, we investigate what changes the energy difference between QW transitions for different Q_C, and we search for the optimal value of the parameter. Usually, the energy of the ground state transition is weakly sensitive to the band offset, while the higher QW levels and the energy difference between them is significantly sensitive. During the identification of QW transitions we take into consideration the intensity of PR resonance and we compare PR resonances to well defined QW transitions in the reference sample. Hence, the reference QW is very useful. Moreover, the observation of nominally forbidden QW transitions is very helpful during the determination of the Q_C parameter. More details about the procedure of matching experiment with theory can be found in [37]. This procedure applied to N-free QWs gives a good agreement with experimental data for m_e^* and Q_C typical for the GaInAs compound.

3.1.2. Determination of the energy level structure by PR spectroscopy. Four subsets of GaInNAs/GaAs single QWs (SQWs) with different indium and nitrogen contents were selected to present the evolution of energy level structure after the introduction of nitrogen atoms into a GaInAs well. The first subset consists of three samples with In content of 28%, QW with 9 nm and nitrogen concentration of AR—0% (reference sample), A1—0.35%, and A2—0.5%. In the second subset there are three samples with In content of 36%, QW width of 7.2 nm and nitrogen concentration of BR—0% (reference sample), B1—0.7%, and B2—1%. The third subset consists of four samples with In content of 41%, QW width 9 nm and nitrogen concentration of CR—0% (reference sample), C1—2%, C2—3.7%, and C3—5.2%. The fourth subset was grown by MOVPE as opposed to the three above grown by MBE. This subset consists of three samples with In content of 34%, QW width of 6.5 nm and nitrogen concentration of DR—0% (reference sample), D1—0.5%, and D2—0.8%. All samples have a $\sim$100 nm thick GaAs capping layer. The last subset was selected in order to compare the quality of MOVPE and MBE GaInNAs/GaAs QWs.

Figures 1 and 2 show room temperature PR spectra of the three subsets of SQWs grown by MBE and one subset of SQWs grown by MOVPE, respectively. Using a GaInAs/GaAs QW as a starting point to study the effect of nitrogen incorporation has several advantages, like for example easier identification of PR resonances of N-containing QWs. All PR spectra are dominated by the GaAs bandgap bulk-like signal above the energy of 1.4 eV. Below this energy the QW-related transitions are observed. The arrows in figure 1 indicate transition energies obtained from the fitting procedure to the PR data using the first derivative Gaussian line-shape (FDGL), the most appropriate form of PR resonances in the case of confined transitions, like those in QWs, at room temperature [38]. The identification of all QW transitions was possible on the basis of calculations described above. The notation *nm*H (L) denotes the transition between the *n*th heavy-hole (light-hole) valence subband and *m*th conduction subband. The resonance at the lowest energy we connect with the 11H transition, which is a fundamental one in such QWs. Besides the 11H transition, the PR spectra show a 11L transition (i.e. the lowest energy transition for light-holes) and transitions between excited QW states: 22H, 12H, 21H, and 32H. The transitions 12H and 21H are forbidden ones but due to the presence of a surface electric field in the structure [39, 40] or other imperfections of the QW it is possible to observe such transitions in PR measurements. The magnitude of the surface electric field in a semi-insulating structure decreases exponentially with the increase of distance to the surface. If a QW is close to the surface its potential can be changed and the symmetry of the QW can be lost [39, 40]. Usually, the surface electric field is very weak and a 100 nm cap is sufficient to

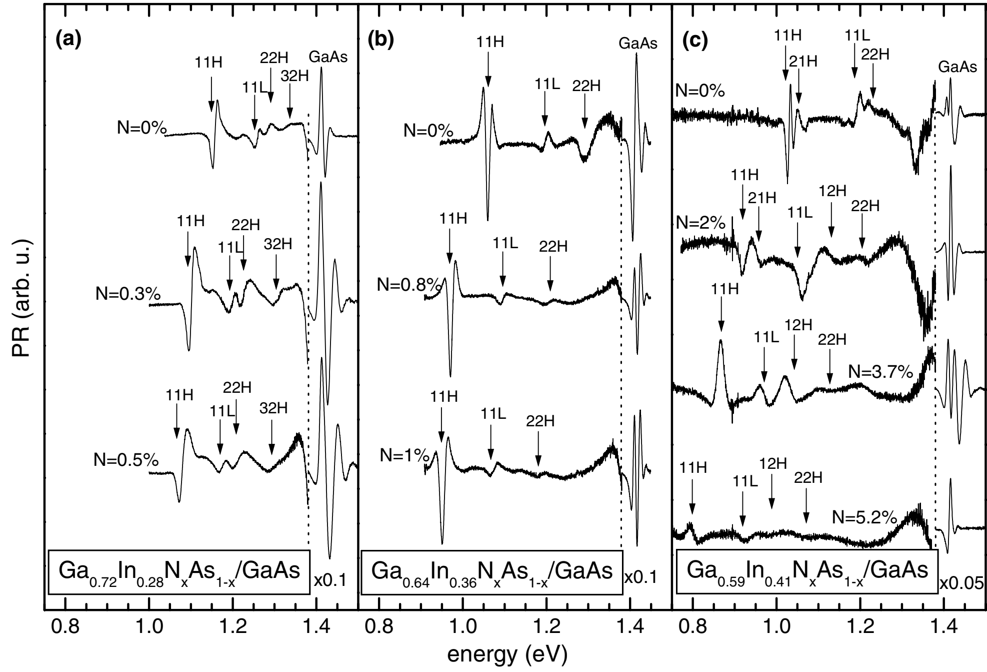

Figure 1. Room temperature PR spectra of $Ga_{0.72}In_{0.28}N_xAs_{x-1}$/GaAs (subset 'A') (a), $Ga_{0.64}In_{0.36}N_xAs_{x-1}$/GaAs (subset 'B') (b), $Ga_{0.59}In_{0.41}N_xAs_{x-1}$/GaAs (subset 'C') SQWs (c) grown by MBE. The samples were grown at WU in Germany.

separate the QW from the surface electric field influence. However, in many cases the surface electric field makes the forbidden transitions observable. Usually in such cases, the Stark shift of QW transitions caused by the surface electric field can be neglected because we are in the limit of very low fields ($F < 1$ kV cm^{-1}). In this regime of electric field the selection rules are changed only while the energies of the QW transitions shift very weakly (below the resolution of the experiment).

In our structures, the existence of a surface electric field is confirmed by the presence of GaAs-related Franz–Keldysh oscillations (FKOs) [41]. The magnitude of the field changes from sample to sample. On the basis of the FKO period, we have estimated that the surface electric field is 14, 21, and 25 kV cm^{-1} for sample A1, A2, A3, respectively; and ~6 kV cm^{-1} for whole subset 'B'. It is 16 kV cm^{-1} for sample C3 and 13, 19, 26 kV cm^{-1} for samples D1, D2, and D3, respectively. The surface electric field was not estimated for samples C1, C2, and C4 due to the absence of FKOs in their spectra. The fact that nominally forbidden transitions are more visible for structures with surface electric field higher than 13 kV cm^{-1} indicates that the surface field changes the square-like profile of the well slightly. It is one of the reasons why the oscillator strength of nominally forbidden transitions is stronger in some cases. Also, other factors like alloy fluctuations and hole wavefunction mixing can influence the selection rules. Such factors seem to be especially important for the subset 'C', i.e. GaIn(N)As layers with a high concentration of In atoms.

Regarding the behaviour of QW transitions after adding nitrogen, it is seen that with the increase in nitrogen content, all the QW transitions shift towards lower energies [42–45]. The analysis of the shift with the increase in nitrogen content seems to be the most interesting

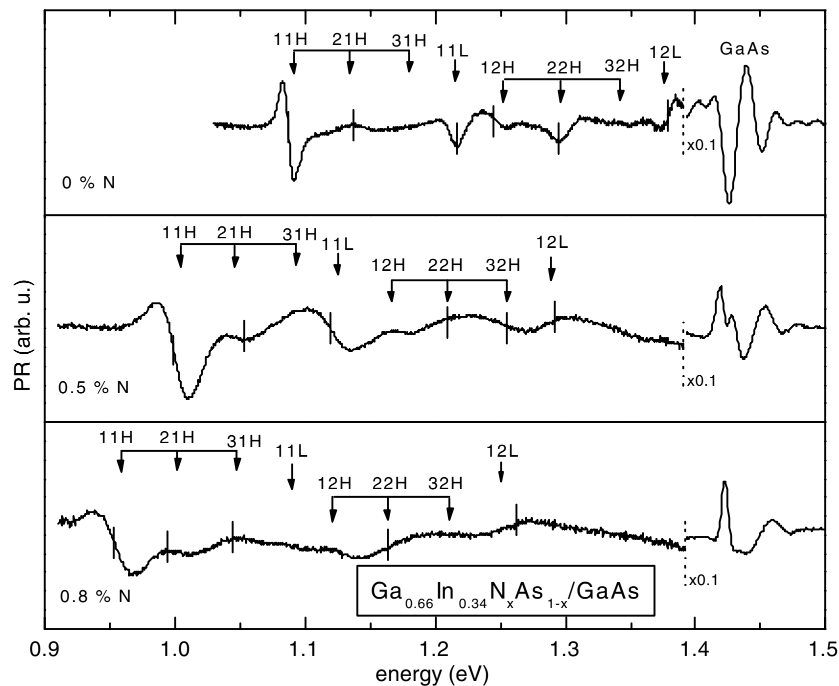

Figure 2. Room temperature PR spectra of $Ga_{0.66}In_{0.34}N_xAs_{x-1}$/GaAs (subset 'D') SQWs grown by MOVPE. The vertical arrows and dash indicate energies obtained from calculations and the fit by FDGL, respectively. The samples were grown at KTH in Sweden.

for the subset 'D', due to a strong PR signal and significant intensity of forbidden transitions. The arrows in figure 2 indicate the transition energies obtained on the basis of calculations. The energies are in good agreement with energies obtained from the fit of the PR data by FDGL (compare the arrows and vertical dash). The energy difference between heavy-hole levels remains almost constant after adding nitrogen atoms. It results from a weak nitrogen-induced change in the QW valence band and negligible changes in the heavy-hole effective mass. The redshift of the QW transitions comes mainly from the shift of electron levels and two factors influence its value. The first is an increase in QW depth and the second is an increase in electron effective mass. The impact of these two factors increases with the increase in nitrogen content. Such significant changes of conduction QW depth and electron effective mass cause the energy difference between electron levels to change significantly after adding nitrogen. For the nitrogen-free SQW the indium content is so high that the band alignment for the light-hole is of type II, leading to indirect light-hole related transitions in real space. The energy difference between fundamental light- and heavy-hole transitions does not change significantly after adding nitrogen. This confirms the fact that the light-hole transitions remain indirect despite the fact that nitrogen atoms reduce the strain in the QW layer and hence also the axial (shear) component of the strain responsible for the valence band splitting. These features evidently show that the incorporation of nitrogen atoms into GaInAs/GaAs QW influences mainly the conduction band, while the valence band remains almost unchanged.

3.1.3. Electron effective mass and conduction band offset determination. In the framework of the BAC model the electron effective mass equals

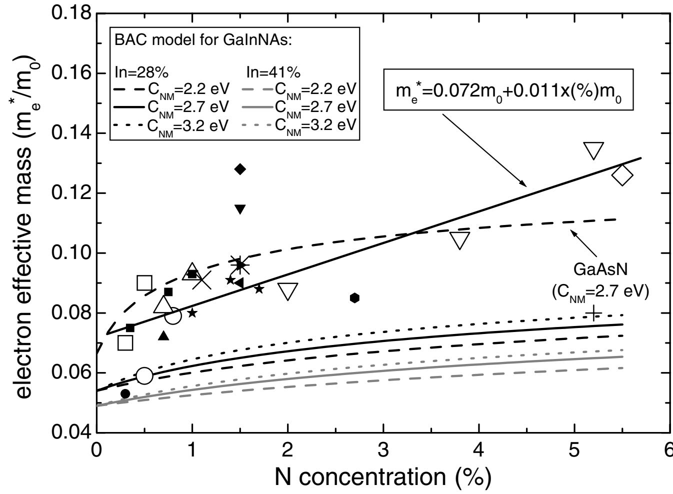

Figure 3. The electron effective mass as a function of N concentration obtained for GaInNAs/GaAs QWs. Open points represent experimental data obtained in this work: □ subset 'A' (28% In); ○ subset 'D' (34% In); △ subset 'B' (36% In); ▽ subset 'C' (41% In); ◇ $Ga_{0.62}In_{0.38}N_{0.053}As_{0.947}$/GaAs SQW (sample analysed in section 3.2 and marked as QW1). The remaining points represent literature data: ● [52]; ■ [49]; ∗ [50]; ▼ 5% In, ▶ 9% In, ★ 14% In, ◆ 14.5% In, ◀ 20% In in $Ga_{1-y}In_yN_xAs_{1-x}$/GaAs MQW [35]; × 25% In, ⬢ 32% In, ▲ 34% In, × 38% In in $Ga_{1-y}In_yN_xAs_{1-x}$/GaAs QW [51].

$$\frac{1}{m_e^*} = \frac{1}{2m_M}\left[1 - \frac{E_M - E_N}{\sqrt{(E_M - E_N)^2 + 4xC_{NM}^2}}\right], \tag{5}$$

where m_M is the electron effective mass in the host matrix (i.e. GaInAs compound). According to equation (5) an increase in the electron effective mass with the increase in nitrogen content takes place. In the case of the BAC electron effective mass, we can find satisfactory agreement with the experiment only for one QW with In = 34% and N = 0.3%, while the agreement drops dramatically for other QWs. In the case of high indium and nitrogen contents, we have obtained QW transitions at higher energies than experimental values. Moreover, other authors [46] have reported a decrease of the C_{NM} matrix element with the increase in indium content. Such behaviour of C_{NM} is intelligible and is rather expected within the BAC model. However, if we take the electron effective mass after the BAC model with C_{NM} less than 2.7 eV (e.g. 2.2 eV), we obtain less agreement with the experimental data. Another approach is to increase the C_{NM} parameter. We have found that this leads to a little better agreement with the experimental data. The increase of the C_{NM} parameter has been also considered by other authors [47], but this approach is rather controversial. Therefore, we decided to fix the C_{NM} parameter for each sample at the level of 2.7 eV and to make the electron effective mass a free parameter.

Figure 3 shows the fitted m_e^* in GaInNAs/GaAs QWs for different indium and nitrogen contents. First, we have found that m_e^* in GaInNAs is bigger than in GaInAs with the same indium concentration. Second, the m_e^* increases with the increase in nitrogen concentration. The values obtained by us are in good agreement with those found for bulk GaInNAs layers by Skierbiszewski *et al* [48] and for GaInNAs/GaAs QWs by other authors [49–52]. The obtained m_e^* agrees with the BAC model only in the range of low indium and nitrogen concentrations.

The variation of the BAC parameters does not change the m_e^* value sufficiently (see the BAC curves in figure 3). Therefore, the electron effective mass cannot be taken after the BAC model if we want to calculate energy levels of GaInNAs/GaAs QWs in the framework of the BAC approximation of GaInNAs bandgap energy. In our approach we have found that in the range of investigated indium and nitrogen contents the influence of indium concentration on m_e^* can be neglected and m_e^* can be approximated by the formula

$$m_e^* = (0.072 + 0.011x)m_0, \tag{6}$$

where x is the nitrogen concentration in %. The obtained formula gives the electron effective mass close to values obtained by the BAC model for GaNAs compounds (see in figure 3). In the case of GaInNAs compounds, an increase in In content leads to a significant decrease of m_e^* within the BAC approach, as seen in figure 3. Such a strong change in m_e^* due to the incorporation of In atoms at the same N content is not observed. The m_e^* increase is a feature which is attributed to the presence of N atoms. The influence of In atoms on m_e^* is not excluded; however, the BAC predictions are reasonably valid. Our results show that the incorporation of 0.3–5.2% of N atoms into GaInAs increases m_e^* by ∼50–130% in comparison to the m_e^* of GaInAs, while the incorporation of as much as 41% of In atoms into GaAs decreases the m_e^* only 25% in comparison to the m_e^* of GaAs. Therefore, the influence of In content on the m_e^* value can be neglected to a first approximation as in equation (6), especially if the scattering of the data is of the order of 20%.

In addition to the m_e^* parameter, the Q_C is a second free parameter in our calculations. This parameter is crucial for the temperature characteristic of laser structures. It is important to have the type I structure with a deep confinement potential for electrons and suitably deep potential for holes. We can determine the conduction band offset on the basis of PR data because QW transitions, especially the excited ones (i.e. 22H, 21H,...), are sensitive to variations of Q_C. In addition, the observation of partially forbidden transitions facilitates the verification of Q_C.

Figure 4 shows the Q_C parameter for the GaInNAs/GaAs SQWs with different indium and nitrogen concentrations obtained in this work (open points) and taken from literature (remaining points). In the case of QWs investigated in this paper the indium content is relatively high ($28\% < \text{In} < 41\%$), and in this range of indium content the Q_C for the GaInAs/GaAs system is almost the same (i.e. $Q_C = 0.8$) [53]. The incorporation of a small quantity of nitrogen atoms ($N < 5\%$) in InGaAs does not change Q_C drastically in comparison with InGaAs material with the same indium concentration. We have obtained the result that with an increase in N concentration to 5%, Q_C increases up to 0.85. Hence, to a first approximation we can assume that Q_C for the GaInNAs/GaAs system is the same as for GaInAs/GaAs one.

To end this section we would like to draw attention to the fact that such additional factors as (i) different nitrogen nearest-neighbour environments, (ii) N-related defects, are not included in the above considerations. This could lead to some discrepancies between the experiment and calculations, because it has been found that these two factors have a significant influence on the bandgap structure of Ga(In)NAs compounds. These aspects are discussed in the following subsections. Moreover, a small difference between the real and determined nitrogen concentration in GaInNAs layer leads to essential changes in the GaInNAs bandgap energy. Therefore, we used the simplest model and we did not vary the BAC parameters. Within this approach two essential results have been confirmed. First, the m_e^* increases after adding nitrogen atoms. Second, the Q_C in the GaInNAs/GaAs system is almost the same as in GaInAs/GaAs one. These two features confirm the fact that nitrogen atoms modify mainly the conduction band.

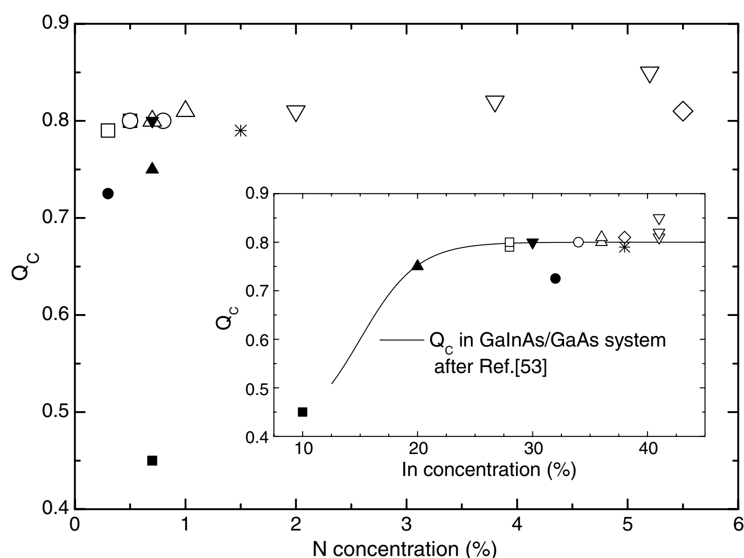

Figure 4. The conduction band offset in GaInNAs/GaAs structure versus N concentration and In concentration (inset). Open points represent experimental data obtained in this work: □ subset 'A' (28% In); ○ subset 'D' (34% In); △ subset 'B' (36% In); ▽ subset 'C' (41% In); ◇ $Ga_{0.62}In_{0.38}N_{0.053}As_{0.947}$/GaAs SQW (sample analysed in section 3.2 and marked as QW1). The remaining points represent literature data: ● [52]; ∗ [50]; ■ 10% In, ▲ 20% In, ▼ 30% In in $Ga_{1-y}In_yN_{0.007}As_{0.993}$/GaAs QW [49].

3.2. The energy level structure of step-like GaInNAs/Ga(In)NAs/GaAs QWs

The step-like GaInNAs/Ga(In)NAs/GaAs QW structures make it possible to achieve 1.3 and 1.55 μm emission at a lower nitrogen and/or indium content. So far, the optical properties of such step-like QWs have mainly been investigated in PL spectroscopy which probes only the ground state transition. Therefore, the energy level structure of the step-like QW system is unknown from the experimental point of view. Also, it is difficult to make theoretical predictions for such a system due to the lack of material parameters for the nitrogen diluted compounds, especially the band offset. Therefore, experimental investigations of the number of confined states in such 1.3 and 1.55 μm laser structures seem to be very interesting from both a fundamental and application point of view. The thorough analysis of this system will be presented elsewhere. In this subsection we show preliminary results of PR investigations for two subsets of step-like QWs tailored at 1.3 and 1.55 μm. Figure 5 shows a comparison of the energy level structure for the three different QW structures. This figure demonstrates the main idea of the step-like QW system and is useful to explain features observed in PR spectra.

Figure 6 shows PR spectra for step-like $Ga_{0.66}In_{0.34}N_xAs_{1-x}/GaN_{0.011}As_{0.989}$/GaAs QW structures with nitrogen content $x = 0.007$ (curve (ii)) and $x = 0.008$ (curve (iv)). In addition, PR spectra of $Ga_{0.66}In_{0.34}N_xAs_{1-x}$/GaAs SQWs, i.e. reference sample with the same nitrogen content ($x = 0.007$ curve (i), and $x = 0.008$ curve (iii)), are shown in figure 6. All these structures were grown by MBE. In the case of the reference SQWs, the 11H and 22H transitions are clearly visible. Also, the 11L transition, with light-hole state having bulk-like (3D) properties, is noticeable. After the introduction of the $GaN_{0.011}As_{0.989}$ step-like barrier the 11H transition shifts to red by 26 and 31 meV for the QW structures with nitrogen content of $x = 0.007$ and 0.008, respectively. The 22H transition shifts to red three times more than

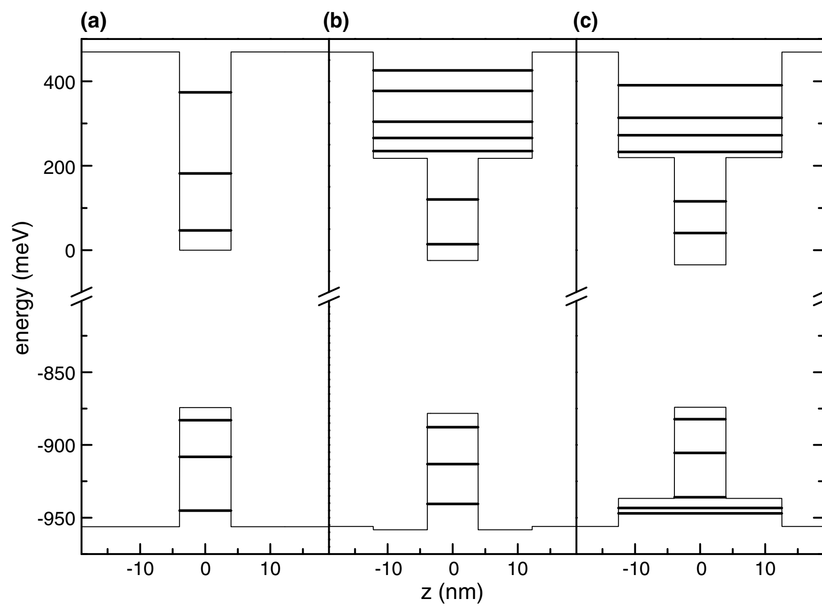

Figure 5. Energy level structures for three different QW systems obtained for some indium and nitrogen contents: (a) GaInNAs/GaAs, (b) GaInNAs/GaNAs/GaAs, and (c) GaInNAs/GaInNAs/GaAs.

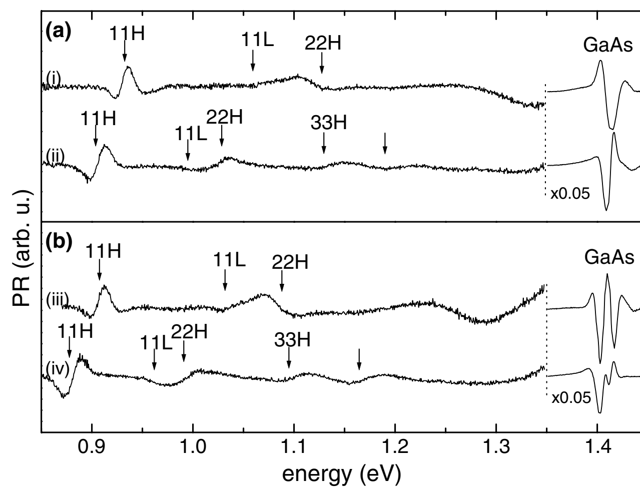

Figure 6. Room temperature PR spectra of step-like QW structures tailored at 1.3 μm. (a): $Ga_{0.64}In_{0.34}N_{0.007}As_{0.993}$(8 nm)/GaAs SQW (reference sample) (i), $Ga_{0.66}In_{0.34}N_{0.007}As_{0.993}$(8 nm)/$GaN_{0.011}As_{0.989}$(8 nm)/GaAs QW structure (ii); (b): (iii) $Ga_{0.64}In_{0.34}N_{0.008}As_{0.992}$(8 nm)/GaAs SQW (reference sample), (iv) $Ga_{0.66}In_{0.34}N_{0.008}As_{0.992}$(8 nm)/$GaN_{0.011}As_{0.989}$(8 nm)/GaAs QW structure. The samples were grown at LPN in France.

the 11H one mainly due to a significant shift of the second electron level. In addition, some resonances have appeared in the PR spectrum above the 22H transition. These transitions are related to a higher than the second electron level. However, we have identified only the 33H transition because on the basis of calculations we have obtained only three confined states

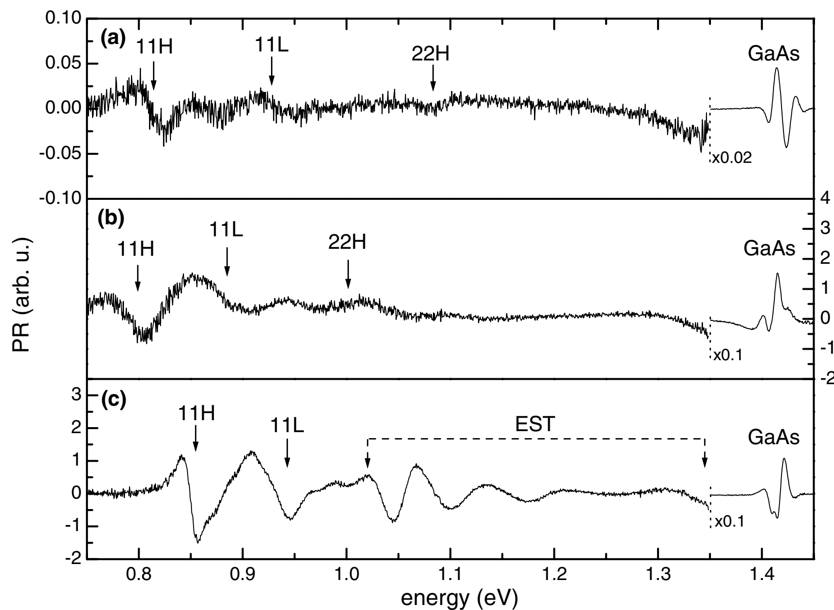

Figure 7. Room temperature PR spectra of QW structures tailored at 1.55 μm: (a) $Ga_{0.62}In_{0.38}N_{0.053}As_{0.947}$(8.2 nm)/GaAs SQW; (b) $Ga_{0.61}In_{0.39}N_{0.025}As_{0.975}$(8.5 nm)/$GaN_{0.04}As_{0.96}$(3.7 nm)/GaAs QW structure; (c) $Ga_{0.63}In_{0.37}N_{0.02}As_{0.98}$(8.2 nm)/$Ga_{0.965}In_{0.035}N_{0.03}As_{0.097}$(8 nm)/GaAs QW structure. The samples were grown at WU in Germany.

for heavy-holes. The energy level structure of the valence QW does not change significantly due to almost flat valence band alignment for the $GaN_{0.011}As_{0.989}$/GaAs system as is seen in figure 6(b). The essential changes in the hole-level structure appear after incorporating the GaInNAs step-like barrier (see figure 5). In this case new confined states appear for holes above the step-like GaInNAs barrier. We have observed transitions related to these levels in the PR spectrum of such a step-like QW structure.

Figures 7(a)–(c) show PR spectra for GaInNAs/GaAs (QW1), GaInNAs/GaNAs/GaAs (QW2) and GaInNAs/GaInNAs/GaAs (QW3) structures, respectively. In the case of the QW1 structure the PR spectrum exhibits features typical for high nitrogen content GaInNAs/GaAs QWs, i.e. a weak PR signal and very broad PR resonances. These two features indicate that these structures are much worse than the previous 1.3 μm QW structures. Similar features are observed for the QW2 structure, but in this case the PR signal is already about one magnitude stronger due to the lower nitrogen content. The other interesting feature is the lack of PR resonance in the 1.1–1.35 eV range despite the fact that new electron levels have appeared after incorporating the GaNAs step-like barrier. We have not observed them because as was mentioned earlier no new confined states for holes have appeared after the introduction of the GaNAs step-like barrier. Due to the selection rules the transitions between the hole subbands with index $n = 1, 2$ and the new electron subbands with index $m = 3, 4, 5, \ldots$ are forbidden. In the case of the QW3 structure, the GaInNAs step-like barrier causes the QW profile to change, as is seen in figure 5, and new confined heavy-hole states with index $n = 3, 4, 5, \ldots$ appear. Hence, in the PR spectrum nmH transitions with index higher than 3 can be observed. Such excited state transitions (EST) are visible in the PR spectrum of the QW3 structure (see figure 7(c)). However, due to the small energy difference between the states confined above the step-like barrier the EST are not resolved and the PR signal looks similar to FKO.

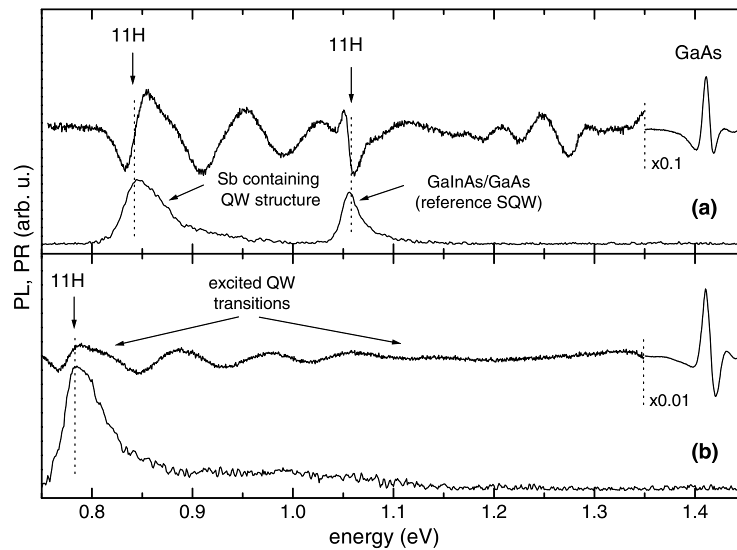

Figure 8. Room temperature PL and PR spectra of Sb-containing Ga(In)NAsSb/GaAs QW structures. (a) Sample with a GaInAs/GaAs SQW (reference QW) and a $Ga_{0.64}In_{0.36}N_{0.012}As_{0.973}Sb_{0.015}$(7 nm)/$GaN_{0.02}As_{0.88}Sb_{0.1}$(5 nm)/GaAs QW structure. (b) Sample with a $Ga_{0.6}In_{0.4}N_{0.015}As_{0.97}Sb_{0.015}$(8 nm)/$GaN_{0.024}As_{0.856}Sb_{0.12}$(5 nm)/GaAs QW structure. The samples were grown at LPN in France.

3.3. The energy level structure of Sb-containing Ga(In)NAs/GaAs QWs

The other approach in order to shift the laser emission of GaInNAs/GaAs system to 1.55 μm is to introduce Sb atoms to the GaInNAs compound [14–16]. This makes it possible to obtain low bandgap energy at a relatively low nitrogen content. In this case the role of nitrogen atoms in GaInNAsSb compounds is the assurance of the deep confinement potential for electrons because for the GaInAsSb/GaAs system the conduction band alignment is between type I and II, depending on the content. An example of PR and PL spectra for an Sb-containing GaInNAs/GaAs system is presented in this subsection.

Figure 8(a) shows PL and PR spectra of MBE-grown samples with a GaInAs/GaAs SQW (reference QW) and a GaInNAsSb/GaNAsSb/GaAs QW structure. In the case of the PL spectrum, it is seen that the integrated PL intensity is bigger for an Sb-containing QW structure. If we neglect the non-radiative processes which are related to defects we should expect an increase in PL intensity for the Sb-containing QW structure due to an increase in the QW depth in comparison to the depth of reference QW. The increase in the broadening of PL emission for the Sb-containing QW structure is mainly attributed to significant alloy fluctuations in GaInNAsSb compounds, because in general it is expected that the five-component compound possesses bigger inhomogeneities than a three-component one.

The PR spectrum of this sample is in good accordance with the PL one. We observe the ground state transitions at the same energy as in the PL spectrum. The broadening of PR resonance is bigger for the Sb-containing structure. Above the 11H transition some excited state transitions are observed. However, a further analysis of the excited state transitions is rather difficult due to a weak knowledge of the material parameters for Sb-containing Ga(In)NAs compounds and the conduction band offset for the Ga(In)NAsSb/GaAs system. In addition, PR resonances related to the excited QW transitions are not defined precisely because alloy inhomogeneities cause a significant broadening of PR resonances.

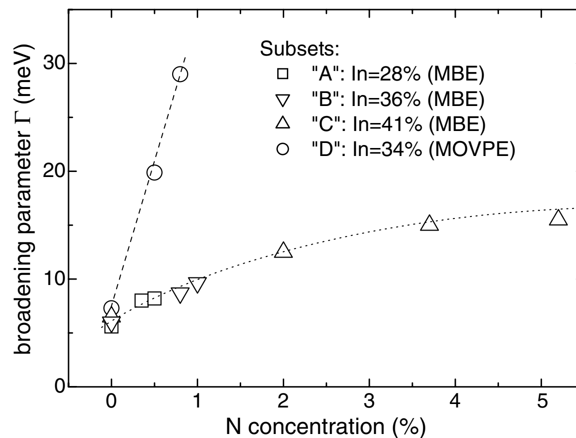

Figure 9. The broadening Γ of PR resonance related to the 11H transition for the subsets 'A', 'B', 'C', and 'D'.

Figure 8(b) shows PL and PR spectra of an MBE-grown sample with an Sb-containing Ga(In)NAsSb/GaAs QW structure which is very similar to the previous one, but this sample is without a reference GaInAs/GaAs SQW. Hence, the analysis of excited QW transitions does not interfere with PR resonances related to other QWs as in the previous sample. In this case in the PL spectrum besides the 11H emission an emission between higher energy levels is observed. The PR spectrum is similar to the PR spectrum of the previous Sb-containing QW structure. The 11H transition observed in PR agrees with that observed in PL. In addition, the PR signal related to excited QW transitions is well correlated with the PL emission observed in this spectral region. The emission band observed between 0.9 and 1.1 eV is a tail-looking emission above the energy of the ground state, but its shape is not an exponential one. Additionally, this disappears with the decrease of temperature (or excitation power at low temperature), which suggests that this band is attributed to a recombination between excited states. Such a recombination is visible because an occupation of excited states by carriers takes place at room temperature. Therefore, we have attributed the PR resonances between 0.85 and 1.2 eV to the excited QW transitions. The PR resonances associated with the excited transitions are not resolved due to the high value of the broadening parameter. These resonances are not resolved either at low temperatures because phonon-related broadening is smaller than the broadening due to alloy inhomogeneities.

3.4. Broadening of PR resonances

The broadening of PR resonance is due to electron–phonon interaction, alloy inhomogeneities and QW width fluctuations. Hence, an analysis of this parameter seems to be very useful while investigating the deterioration of optical quality due to the incorporation of nitrogen atoms in GaInAs compounds.

Figure 9 shows the broadening parameter of the 11H transition for the QWs analysed in section 3.2. We have observed that the broadening of PR resonance increases with the increase in nitrogen content for all subsets of QWs. The increase in the broadening parameter is mainly attributed to an increase in GaInNAs alloy inhomogeneities due to the introduction of nitrogen atoms. We assume that other factors, which also lead to a broadening of PR resonance, have similar contributions to the total PR broadening for each QW. The other factors originate from

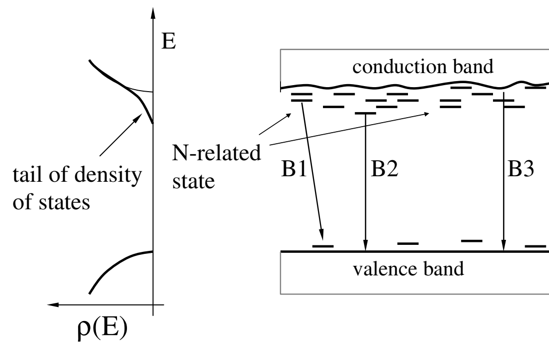

Figure 10. Bandgap diagram of the GaInNAs compound. Only the fluctuations in the conduction band have been assumed.

electron–phonon interactions and QW width fluctuations. At the fixed temperature and the comparable roughness of QW interfaces we can assume that the contribution of the other factors to the increase of the broadening parameter is negligible.

The increase in inhomogeneities is due to the tendency of nitrogen atoms to cluster (i.e. the creation of nitrogen pairs or other clusters) [32] and the formation of N-related defect states (nitrogen interstitials, Ga vacancy complexes) [54]. Moreover, the band structure of GaInNAs compounds strongly depends on the nitrogen nearest-neighbour environment [30]. The mentioned phenomena lead to bandgap fluctuations and to a tail of the density of states (DOS) as in figure 10. This scheme of band structure assumes unusual bandgap fluctuations. Usually, alloy content fluctuations lead to bandgap fluctuations where both conduction and valence bands possess local minima. Nitrogen content fluctuations in III–V-N compounds, like GaNAs, GaInNAs, and GaNAsSb, lead to a specific variation in the energy bandgap. In this case, the variation in the bandgap is mainly due to the changes of a conduction band, while the changes of a valence band can be neglected [43, 55]. Such behaviour is simple to explain within the BAC model which assumes that the resonant nitrogen level interacts only with the conduction band of the host matrix (i.e. the compound without nitrogen atoms). The magnitude of the interaction strongly depends on the nitrogen content, and a small fluctuation in nitrogen content leads to a significant fluctuation in the conduction band minima. Also, the change of GaInNAs bandgap due to the change in the nitrogen nearest-neighbour environment leads to fluctuations in conduction band minima only. Moreover, a non-homogeneous distribution of the N-related defects, which are located close to a conduction band, also affects only the conduction band.

On the basis of such a model it is easy to explain the unusually broad PR resonance and high value of Stokes shift for QWs with smooth interfaces. Hence, within an assumed model, the increase in the broadening parameter indicates an increase in the magnitude of conduction band fluctuations and/or an increase of DOS tails. It is equivalent to the redistribution of nitrogen atoms between different nitrogen nearest-neighbour environments and/or the increase in the number of N-related defects.

In the case of MOVPE-grown QWs, the Γ parameter increases by a factor of 1.2, 2.4, and 3.0 for QWs with 0 (reference QW), 0.5, and 0.7% nitrogen content, respectively. The bigger broadening obtained in the case of MOVPE structures can be understood because this epitaxial growth method is worse than the MBE, in general. But we have concluded that the Γ increase has to have an additional origin, because these structures posses rather good optical properties and the degree of Γ increase is significantly larger for N-containing QWs than for N-free QWs

(1.2 versus 2.2 and 3.0). We are convinced of the good quality of these QWs because the MOVPE process was refined, and all these QWs were *in situ* annealed for 10 min at 680 °C. This procedure has reduced the point defects and improved the optical properties significantly. Therefore, we have concluded that an additional phenomenon is responsible for such a large value of the broadening. The additional phenomenon is associated with the presence of different nitrogen nearest-neighbour environments. These different environments of nitrogen atoms appear due to annealing (this phenomenon is discussed in detail in section 3.5). Within the assumed bandgap diagram (see figure 10) the coexistence of different nitrogen nearest-neighbour environments leads to bigger fluctuations in the conduction band [43]. In the case of MBE-grown QWs different environments of N atoms are probably not present, because these structures were not annealed. The other environments of N atoms are expected mainly for annealed QWs. So far, Raman scattering [56] and infrared transmission [57–59] studies have shown that the annealing process leads to the formation of N–In bonds instead of N–Ga ones, i.e. the change of nitrogen nearest-neighbour environments.

3.5. PR investigations of annealing effect

The N-containing structures are usually annealed in order to reduce N-related defects. It significantly increases the PL efficiency but it simultaneously shifts the bandgap energy to blue [17–19]. The origin of the blueshift is still controversial. In the case of GaInNAs compounds it is reasonably established that the increase in bandgap energy after RTA is due to the change in nitrogen nearest-neighbour environment from Ga-rich to In-rich [30, 60]. However, it is not excluded that other phenomena affect the bandgap energy. Especially, that a blueshift of the bandgap energy has been observed for post-grown annealed GaNAs compounds [55, 61]. In this case, the absence of indium atoms supports the other phenomena. Another phenomenon which could be responsible for the blueshift of the bandgap energy is a reduction of the DOS tail by post-grown annealing [55]. It is quite well established that post-grown annealing leads to a reduction of N-related defects. Hence, it should influence the DOS tail and thereby the bandgap energy. These issues are considered in this subsection.

3.5.1. Post-growth annealing of (Ga, In) (N, As, Sb) layers. Figures 11(a)–(c) show PL and PR spectra for as-grown and annealed $GaN_{0.02}As_{0.98}$, $Ga_{0.95}In_{0.05}N_{0.2}As_{0.98}$, and $GaN_{0.02}As_{0.9}Sb_{0.08}$ layers, respectively. It is noted that the three layers possess different strains. The GaNAs ternary layer is tensilely strained ($\varepsilon = -7.9 \times 10^{-3}$) and its PL and PR spectra, shown in figure 11(b), clearly exhibit two structures which are related to the heavy- and light-hole splitting. The GaInNAs layer is almost lattice-matched to the GaAs substrate ($\varepsilon = -0.7 \times 10^{-3}$), and is thereby unstrained. In consequence, we do not see any splitting of the valence band in this sample, and a single structure is observed on the PR spectra. In the case of GaNAsSb layers we have found that the layer is compressively strained ($\varepsilon = 4.5 \times 10^{-3}$). Such strain leads to an essential splitting of the valence bands. The line-shape of the PR spectrum confirms the splitting. However, the splitting is not considered in this paper.

In the case of PR measurements, which are not sensitive to defect-related states, we observe absorption between extended states. At room temperature these resonances are associated with the band-to-band absorption. The negligible Stokes shift between emission and absorption (i.e. PL and PR transitions) indicates that the band-to-band recombination of free carriers is dominant in PL at room temperature.

A piece of every sample has been annealed at the same conditions, i.e. at 750 °C for 10 min. We carefully analysed the structural properties of the samples, comparing their characteristics before and after annealing. High resolution x-ray diffraction (HRXRD) did not reveal any

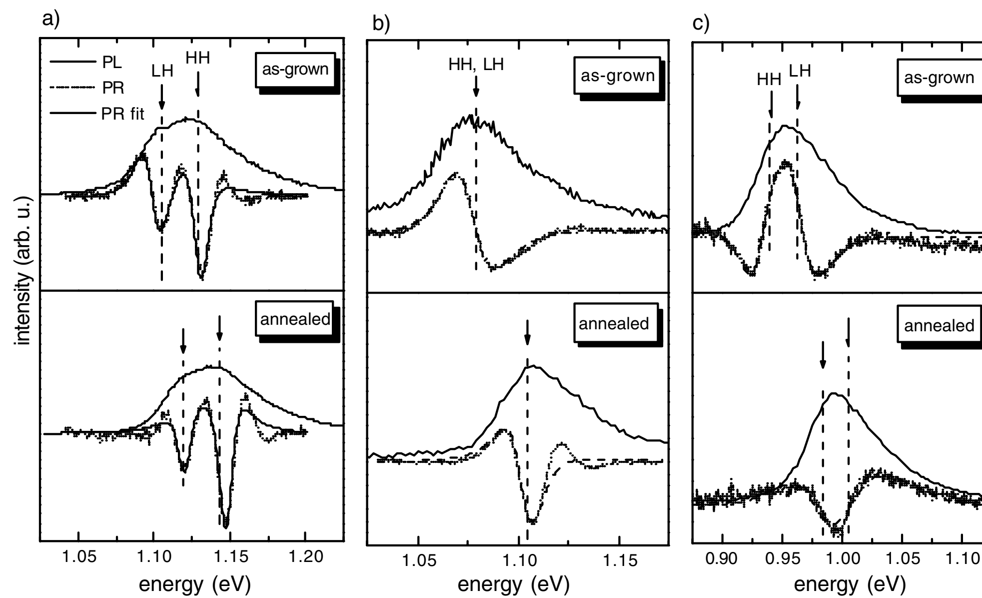

Figure 11. Room temperature PL and PR spectra of as-grown and annealed $GaN_{0.02}As_{0.98}$ (a), $Ga_{0.95}In_{0.05}N_{0.2}As_{0.98}$ (b), and $GaN_{0.02}As_{0.9}Sb_{0.08}$ layers (c). The PR spectra are fitted by FDGL curves. The samples were grown at LPN in France.

changes in the average composition of these two samples. In addition, transmission electron microscopy (TEM) did not show any significant alloy fluctuations, suggesting that composition uniformity was not affected by annealing. We therefore consider that the compound content is the same before and after annealing. Moreover, it has to be noted that the transition energies are not sensitive to possible interdiffusion at the interfaces, since the layer is thick enough to cause negligible quantum confinement (bulk-like case).

The room temperature PL and PR spectra for annealed layers are presented in the bottom part of figure 11. We have found that the blueshift of the bandgap energy equals 20, 27, and 54 meV for the GaNAs, GaInNAs, and GaNAsSb layers, respectively. These shifts cannot be attributed to an atom out-diffusion, because it has been excluded by structural investigations. Hence, this phenomenon has been attributed to the effect of the change in nitrogen nearest-neighbour environment and the effect of the reduction of the DOS tail [55]. Both effects appear as the result of the annealing, and their magnitude depends on the conditions of the annealing. The effect of the nitrogen nearest-neighbour environment is important only for the GaInNAs compound while for the GaNAs compound this effect is absent. Hence, the blueshift for this compound is smaller than for the GaInNAs one. In the case of the GaNAsSb layer the effect of the nitrogen environment also can be important. However, no theoretical predictions have been done so far. The effect of the reduction of the DOS tail due to annealing can be different for every sample because the DOS tail usually changes from sample to sample. Such a tail is the origin of the effect of bandgap shrinkage. The post-growth annealing reduces the shrinkage effect due to the reduction of the DOS tail. It leads to a blueshift of the bandgap energy. Within the bandgap diagram shown in figure 10 it is proposed that N-related defects create energy levels close to the conduction band and they are the origin of the DOS tail. The DOS tail of the valence band is neglected in these considerations because the theoretical predictions show that N-related defects form energy levels only near the conduction band [32]. In our case the presence of a DOS tail was strongly manifested in low temperature PL spectra [55].

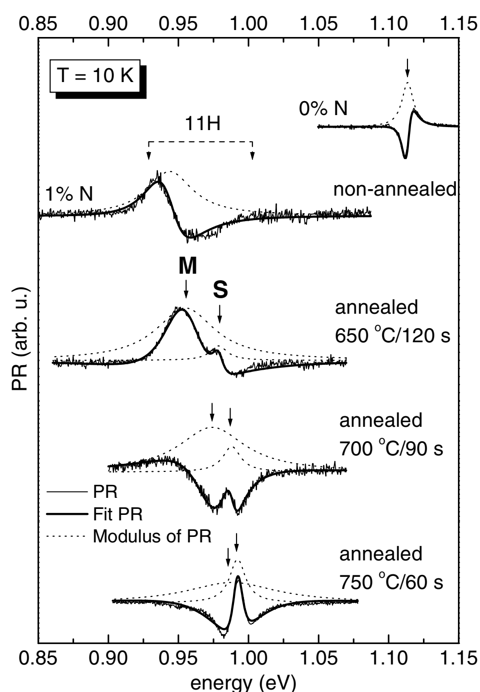

Figure 12. Low temperature PR spectra of as-grown and annealed $Ga_{0.64}In_{0.36}N_{0.01}As_{0.99}$/GaAs SQWs together with fitted curves. The samples were grown at WU in Germany.

Finally we would like to draw attention to the fact that the time of annealing was relatively long while the temperature of annealing could be not high enough for essential changes in the nitrogen nearest-neighbour environment, i.e. to obtain an In-rich environment. In general, an interplay between the two effects is expected for the GaInNAs system. We believe that the interplay depends on both the sample quality and the annealing conditions. For example, we have observed that for an annealing time of 60 s and a temperature higher than 750 °C the change in nitrogen nearest-neighbour environment is the dominant effect for GaInNAs compounds.

3.5.2. Post-growth annealing of GaInNAs/GaAs QWs: the effect of the nitrogen nearest-neighbour environment and atom interdiffusion across QW interfaces. A blueshift of the QW emission due to RTA has been reported many times for GaInNAs/GaAs QW. In this subsection we present the PR investigations of this phenomenon. The 7 nm thick $Ga_{0.64}In_{0.36}N_{0.01}As_{0.99}$/GaAs SQW structures grown by MBE were selected for this research. These SQW structures were annealed under different temperature and duration conditions. Samples annealed at 650 °C for 120 s, at 700 °C for 90 s, and at 750 °C for 60 s are presented in this subsection. In the case of the high quality GaInNAs layer (i.e. the layer with low nitrogen content) the influence of the DOS tail can be neglected. The negligible presence of a DOS tail in these SQWs is confirmed by the small enhancement of the PL intensity after annealing. Such a behaviour of PL intensity indicates that before annealing the number of defects is low. Therefore in this case, the DOS tail is neglected, and only the effect of atom interdiffusion across QW interfaces and the effect of nitrogen nearest-neighbour environment are considered.

Figure 12 shows PR spectra for the SQWs investigated in the vicinity of the heavy-hole ground state transition (11H) recorded at 10 K together with curves approximating these

spectra [20, 21], and the modulus of particular PR resonances. For the non-annealed SQW a rather broad signal is observed. It could be suggested that such a broad contour is connected with multiple QW-related excitonic transitions. However, it fits with a single PR resonance reasonably well and no more transitions can be distinguished in this case. The broadening parameter obtained equals 19 meV and is approximately four times greater than that obtained for the reference N-free sample (see figure 12). In the case of the annealed structures, a splitting of the fundamental transition is clearly visible, hence the PR spectra have been fitted using two resonances. The transition at the lower energy (labelled 'M') has a broadening parameter comparable with the non-annealed SQW, while the second one (labelled 'S') has almost the same parameter as in the case of the reference structure (see figure 12). Such a pair of transitions cannot be explained by a superposition of heavy- and light-hole related features. The fundamental light-hole transition was observed at a much higher energy (see section 3.1). Such a splitting of the 11H transition has previously been observed for MOVPE-grown GaInNAs/GaAs QWs, and has been attributed to the various nitrogen nearest-neighbour environments in the GaInNAs alloy [30]. In accordance with the calculations of Klar *et al* [30], the fundamental transition can be split into five. In the case of $Ga_{0.64}In_{0.36}As_{0.99}N_{0.01}$/GaAs QWs the energy difference between the lowest energy (4Ga) and highest energy (4In) transition is about 50 meV, and the difference between neighbouring transitions is approximately equal (10 meV in this case). The range of 50 meV is illustrated in figure 12 by a dashed line between the arrows. It may be assumed that the broadening parameter for each of these five possible transitions is comparable and is likely to be slightly larger than for the reference SQW (due to some extra disorder caused by the fourth component of the alloy). Wherever the energy difference between consecutive transitions is similar to the broadening parameter, the individual PR resonances are usually not distinguishable (as for the non-annealed sample). However, if one transition is amplified and has a significantly higher intensity (PR amplitude) than the others, then this resonance should be visible against the background of the other resonances. Such a case is observed in our annealed QWs. On the basis of its location this second resonance has been attributed to the 1Ga3In nitrogen configuration. This agrees very well with the calculations of Kim and Zunger using Monte Carlo simulations of a GaInNAs supercell [62]. They showed that the configuration of one gallium and three indium atoms around a nitrogen atom is the most favourable. During a process of fast growth of the quaternary layer the 4Ga configuration, with strongly strained Ga–N bonds, is most frequently obtained. The annealing procedure allows a (so-called short range order) redistribution of atoms in the crystal lattice and the system tends to one with minimal energy, namely the most favourable atom configuration (1Ga3In in this case). The final distribution should depend on the parameters of the RTA process. Klar *et al* [30] observed that as the RTA temperature increases the higher energy transitions (related to more indium atoms) start to dominate in the PR spectrum. We are convinced that, in our study, the second resonance for all the annealed structures is associated with the 1Ga3In nitrogen configuration, but then its energy should be independent of the annealing conditions. We observe that the 'S' feature intensity (PR amplitude) increases with the rise in the annealing temperature (a higher RTA temperature favours the most probable configuration), whereas both the 'M' and 'S' PR transitions shift to higher energies when the annealing temperature increases. The latter shift can be attributed to the changes in the shape of the QW due to atom diffusion across the QW interface. The analysis of the morphology and composition of such QWs has shown that a very thin intermediate layer can be created at the GaInNAs/GaAs interface [63], which can be smoothed out after annealing. Previous TEM measurements have confirmed that the interdiffusion of interfaces after annealing is very weak [19], but despite the fact that this effect is significantly weaker than for example in InGaAsP/InP structures, where it plays a crucial role [64, 65], it cannot be neglected. Annealing

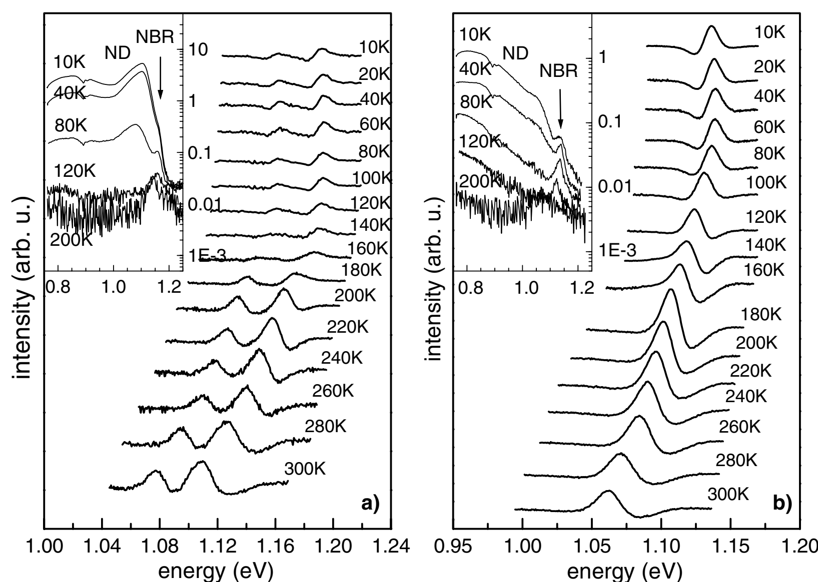

Figure 13. The temperature dependence of the PR spectrum for $GaN_{0.02}As_{0.98}$ (a) and $Ga_{0.95}In_{0.05}N_{0.02}As_{0.98}$ (b) layers. The insets show PL spectra.

causes the potential well to be smoothed (to a round well instead of a square well) and hence the energy level shifts, which results in a blueshift of the ground state optical transition. In the case of a diffusion length of about 2 ML (≈0.5 nm) the transition energy of such a QW as ours can shift by even more than 10 meV [66]. Therefore, the total annealing-induced blueshift of the ground state transition is caused by two effects: changes in the nearest-neighbour configuration of nitrogen atoms and changes in the QW profile. However, as can be seen in figure 12, the value of the energy shift is not the same for the 'M' and 'S' features (the 'M' line shifts more rapidly as the annealing temperature increases). If we compare the values of this energy difference for each line between the samples annealed at 650 and 750 °C, we obtain 13 and 31 meV for the 'S' and 'M' transitions, respectively. The first shift is caused entirely by changes in the QW profile (assuming that this is related to the 1Ga3In configuration), whereas the latter must be related to some additional effect. We have to remember that this 'M' feature is multiresonance. Therefore, if the individual resonances are redistributed after annealing in such a way that the higher energy ones became more intensive, then this results in an apparent shift of the whole 'M' feature. This explanation of the annealing-induced blueshift of the QW transition was also supported by the PL experiment [60].

3.6. Manifestation of the carrier localization effect in PR spectroscopy

The carrier localization effect has been observed many times in PL spectroscopy. Recently this effect has been also confirmed by PR spectroscopy [67, 68]. In the case of PR the carrier localization effect which is present at low temperatures leads to a decrease of PR signal due to a weakness of the band bending photomodulation.

Figures 13(a) and (b) show the temperature dependence of the PR spectrum for the GaNAs and GaInNAs samples which are analysed in section 3.5. Figure 14 shows the temperature dependence of the transition intensity obtained by using a Kramers–Kronig analysis [69] of the PR spectra. A decrease of transition intensity with the decrease of temperature is observed for

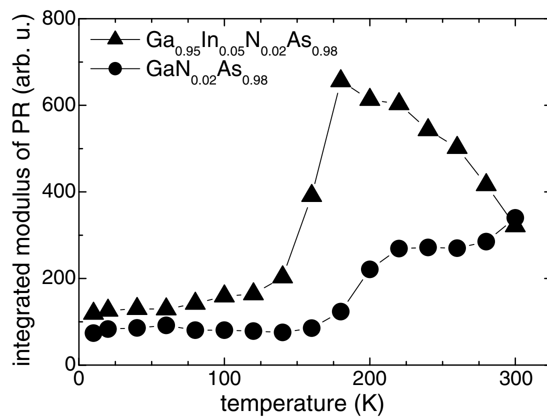

Figure 14. The integrated modulus of the PR obtained from a Kramers–Kronig analysis versus temperature. In the case of $GaN_{0.02}As_{0.98}$ layers the presented intensities are the sum of LH and HH transition intensities.

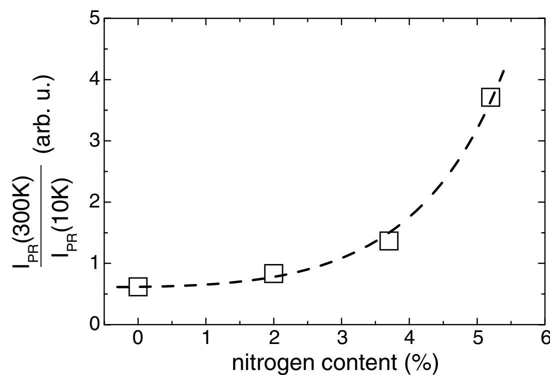

Figure 15. The ratio of room (300 K) and low temperature (10 K) PR amplitudes versus the nitrogen content for the series of $Ga_{0.59}In_{0.41}N_xAs_{1-x}$/GaAs SQWs.

the GaNAs and GaInNAs layers. Such an unusual behaviour of the PR signal is not observed for high-quality semiconductor compounds, like for example GaAs or InP. In the case of GaNAs and GaInNAs compounds the PR signal at low temperatures decreases, because carriers induced by the pump beam are immediately localized on some potential fluctuations and cannot move. Such a phenomenon weakens the modulation of the built-in electric field. With an increase in temperature the thermal energy increases and the localization energy can be exceeded, which is reflected in the possibility for carriers to move. Such behaviour induces an increase in the modulation efficiency, because moving carriers allow a change in the built-in electric field.

A decrease in photomodulation efficiency at low temperatures due to the carrier localization effect has been also observed for GaInNAs/GaAs QW structures [68]. We have found that with the increase in nitrogen content the effect of carrier localization is enhanced and the PR signal at low temperature decreases drastically. An example of this effect is shown in figure 15. This figure shows the ratio of the transition intensity at 300 and 10 K for the subset 'C' of SQWs. It is clearly visible that with the increase in nitrogen content the ratio rises due to the decrease of PR intensity at 10 K.

The carrier localization effect is usually observed for nitrogen-diluted GaAs and GaInAs layers and QWs [67, 68]. Hence, the low temperature PR measurements could be limited,

especially for structures with high nitrogen content, because with the increase in nitrogen mole fraction the carrier localization effect is stronger and makes the band bending photomodulation difficult.

4. Summary

We have presented the power of PR spectroscopy in the investigation of the energy level structure and optical quality of GaInNAs-based QW systems. The electron effective mass and conduction band offset have been determined on the basis of PR data. In addition, the energy level structure for the step-like GaInNAs/Ga(In)NAs/GaAs QW structures tailored at 1.3 and 1.55 μm and the Sb-containing Ga(In)NAs/GaAs QW structures have been analysed using PR spectroscopy. Moreover, PR spectroscopy, as an absorption-type experiment which is not directly sensitive to defect state, has been applied to explain the annealing-induced blueshift of the bandgap energy in bulk layers (GaNAs, GaInNAs, and GaNAsSb) and GaInNAs/GaAs SQWs.

Acknowledgments

The research at Wroclaw University of Technology was supported by EC/EU IST project GIFT no IST-1999-12700, by the Committee for Scientific Research in Poland under Grant no 4 T11B 008 23 and Grant no 2P03B 108 25, and by the Centre for Advanced Materials and Nanotechnology, Wroclaw University of Technology, Wroclaw, Poland. One of the authors (R Kudrawiec) acknowledges the financial support from the Foundation for Polish Science.

References

[1] Kondow M, Uomi K, Niwa A, Kikatani T, Watahiki S and Yazawa Y 1996 *Japan. J. Appl. Phys.* **35** 1273
[2] Reinhardt M, Fischer M, Kamp M, Hofmann J and Forchel A 2000 *IEEE Photon. Technol. Lett.* **12** 239
[3] Steinle G, Riechert H and Egorov A Yu 2001 *Electron. Lett.* **37** 93
[4] Fischer M, Gollub D and Forchel A 2002 *Japan. J. Appl. Phys.* 1 **41** 1162
[5] Li W, Jouhti T, Peng C S, Konttinen J, Laukkanen P, Pavelescu E-M, Dumitrescu M and Pessa M 2001 *Appl. Phys. Lett.* **79** 3386
[6] Kawaguchi M, Miyamoto T, Gouardes E, Schlenker D, Kondo T, Koyama F and Iga K 2001 *Japan. J. Appl. Phys.* 2 **40** L744
[7] Harris J S Jr 2002 *Semicond. Sci. Technol.* **17** 880
[8] Bian L F, Jiang D S, Lu S L, Huang J S, Chang K, Li L H and Harmand J C 2003 *J. Cryst. Growth* **250** 339
[9] Fischer M, Gollub D, Reinhardt M, Kamp M and Forchel A 2003 *J. Cryst. Growth* **251** 353
[10] Gupta J A, Barrios P J, Aers G C, Williams R L and Wasilewski Z R 2003 *Solid-State Electron.* **47** 399
[11] Li L H, Patriarche G, Lemaitre A, Lemaitre L, Largeau L, Travers L and Harmand J C 2003 *J. Cryst. Growth* **251** 403
[12] Pavelescu E-M, Peng C S, Jouhti T, Konttinen J, Li W, Pessa M, Dumitrescu M and Spanulescu S 2002 *Appl. Phys. Lett.* **80** 3054
[13] Pavelescu E-M, Jouhti T, Peng C S, Li W, Konttinen J, Dumitrescu M, Laukkanen P and Pessa M 2002 *J. Cryst. Growth* **241** 31
[14] Ungaro G, Le Roux G, Teisser R and Harmand J C 1999 *Electron. Lett.* **35** 1246
[15] Li L H, Sallet V, Patriarche G, Largeau L, Bouchoule S, Travers L and Harmand J C 2003 *Appl. Phys. Lett.* **83** 1298
[16] Bank S, Ha W, Gambin V, Wistey M, Yuen H, Goddard L, Kim S and Harris J S Jr 2003 *J. Cryst. Growth* **251** 367
[17] Pan Z, Miyamoto T, Sato S, Koyama F and Iga K 1999 *Japan. J. Appl. Phys.* 1 **38** 1012
[18] Shirakata S, Kondow M and Kitatani T 2002 *Appl. Phys. Lett.* **80** 2087
[19] Albrecht M, Grillo V, Remmele T, Strunk P, Egorov A Yu, Dumitras Gh, Riechert H, Kaschner A, Heitz R and Hoffmann A 2002 *Appl. Phys. Lett.* **81** 2719

[20] Pollak F H 1994 *Handbook on Semiconductors* vol 2, ed T S Moss (Amsterdam: Elsevier) pp 527–635
[21] Misiewicz J, Sitarek P, Sek G and Kudrawiec R 2003 *Mater. Sci.* **21** 263
[22] Hammar M, Asplund C, Sundgren P, Mogg S, Christiansson U, Aggerstam T, Oscarsson V, Runnstroem C, Oedling E and Malmquist J 2003 *Proc. SPIE* **4942** 137
[23] Harmand J C, Ungaro G, Largeau L and Le Roux G 2000 *Appl. Phys. Lett.* **77** 2482
[24] Shan W, Walukiewicz W, Ager J W III, Haller E E, Geisz J F, Friedman D J, Olson J M and Krutz S R 1999 *Phys. Rev. Lett.* **82** 1221
[25] Suemune I, Uesugi K and Walukiewicz W 2000 *Appl. Phys. Lett.* **77** 3021
[26] Chtourou R, Bousbih F, Ben Bouzid S, Charfi F F, Harmand J C, Ungaro G and Largeau L 2002 *Appl. Phys. Lett.* **80** 2075
[27] Polimeni A, Capizzi M, Geddo M, Fischer M, Reinhardt M and Forchel A 2001 *Phys. Rev.* B **63** 195320
[28] Kudrawiec R, Sek G, Misiewicz J, Li L H and Harmand J C 2003 *Solid State Commun.* **129** 353
[29] Lindsay A and O'Reilly E P 1999 *Solid State Commun.* **112** 443
[30] Klar P J, Grüning H, Koch J, Schäfer S, Volz K, Stolz W, Heimbrodt W, Kamal Saadi A M, Lindsay A and O'Reilly E P 2001 *Phys. Rev.* B **64** 121203(R)
[31] Duboz J-Y, Gupta J A, Wasilewski Z R, Ramsey J, Williams R L, Aers G C, Riel B J and Sproule G I 2002 *Phys. Rev.* B **66** 085313
[32] Kent P R C, Bellaiche L and Zunger A 2002 *Semicond. Sci. Technol.* **17** 851 and reference therein
[33] Bastard G 1992 *Wave Mechanics Applied to Semiconductor Heterostructures* (Paris: Les Editions de Physique)
[34] Pikus G E and Bir G L 1960 *Sov. Phys.—Solid State* **1** 136
Pikus G E and Bir G L 1960 *Sov. Phys.—Solid State* **1** 1502
[35] Heroux J B, Yang X and Wang W I 2002 *J. Appl. Phys.* **92** 4361
[36] Vurgaftman I and Meyer J R 2003 *J. Appl. Phys.* **94** 3675 and reference therein
[37] See for example, Hall D J, Hosea T J C and Button C C 1998 *Semicond. Sci. Technol.* **13** 302 and reference therein
[38] Glembocki O J 1990 *Proc. SPIE* **1286** 2
[39] Kudrawiec R, Sek G, Sitarek P, Ryczko K, Misiewicz J, Wang T and Forchel A 2004 *Thin Solid Films* **450** 71
[40] Sek G, Ryczko K, Misiewicz J, Bayer M, Wang T and Forchel A 2001 *Acta Phys. Pol.* A **100** 417
[41] Shen H and Dutta M 1995 *J. Appl. Phys.* **78** 2151
[42] Sek G, Ryczko K, Misiewicz J, Fischer M, Reinhardt M and Forchel A 2000 *Thin Solid Films* **380** 240
[43] Kudrawiec R, Sek G, Ryczko K, Misiewicz J, Sundgren P, Asplund C and Hammar M 2003 *Solid State Commun.* **127** 613
[44] Misiewicz J, Sitarek P, Ryczko K, Kudrawiec R, Fischer M, Reinhardt M and Forchel A 2003 *Microelectron. J.* **34** 737
[45] Misiewicz J, Sek G, Kudrawiec R, Ryczko K, Gollub D, Reithmaier J P and Forchel A 2003 *Microelectron. J.* **34** 351
[46] Hetterich M, Grau A, Egorov A Yu and Reichert H 2003 *J. Appl. Phys.* **94** 1810
[47] Sun H D, Dawson M D, Othman M, Yong J C L, Rorison J M, Gilet P, Grenouillet L and Million A 2003 *Appl. Phys. Lett.* **82** 376
[48] Skierbiszewski C, Perlin P, Wisniewski P, Knap W, Suski T, Walukiewicz W, Shan W, Yu K M, Ager J W, Haller E E, Geisz J F and Olson J M 2000 *Appl. Phys. Lett.* **76** 2409
[49] Hetterich M, Dawson M D, Egorov A Yu, Bernklau D and Riechert H 2000 *Appl. Phys. Lett.* **76** 1030
[50] Pan Z, Li L H, Lin Y W, Sun B Q, Jiang D S and Ge W K 2001 *Appl. Phys. Lett.* **78** 2217
[51] Baldassarri Höger von Högersthal G, Polimeni P, Masia M, Bissiri M, Capizi M, Gollub D, Fischer M and Forchel M 2003 *Phys. Rev.* B **67** 233304
[52] Choulis S A, Hosea T J C, Tomic S, Kamal Saadi M, Admas A R, O'Reilly E P, Weinstein B A and Klar P J 2002 *Phys. Rev.* B **66** 165321
[53] Joyce M J, Johnson M J, Gal M and Usher B F 1988 *Phys. Rev.* B **38** 10978
[54] Li W, Pessa M, Ahlgren T and Decker J 2001 *Appl. Phys. Lett.* **79** 1094
[55] Kudrawiec R, Sek G, Misiewicz J, Li L H and Harmand J C 2004 *Eur. Phys. J.* B at press
[56] Wagner J, Geppert T, Kohler K, Ganser P and Herres N 2001 *J. Appl. Phys.* **90** 5027
[57] Kitatani T, Kondow M and Kudo M 2001 *Japan. J. Appl. Phys.* **40** L750
[58] Kurtz S R, Klem J F, Allerman A A, Sieg R M, Seager C H and Jones E D 2001 *Appl. Phys. Lett.* **80** 1379
[59] Kurtz S, Webb J, Gedvilas L, Friedman D, Geisz J, Olson J, King R, Joslin D and Karam N 2000 *Appl. Phys. Lett.* **78** 748
[60] Kudrawiec R, Sek G, Misiewicz J, Gollub D and Forchel A 2003 *Appl. Phys. Lett.* **83** 2772
[61] Grenouillet L, Bru-Chevallier C, Guillot G, Gilet P, Ballet P, Duvaut P, Rolland G and Million A 2002 *J. Appl. Phys.* **91** 5902

[62] Kim K and Zunger A 2001 *Phys. Rev. Lett.* **86** 2609
[63] Patriarche G, Largeau L, Harmand J C and Gollub D 2004 *Appl. Phys. Lett.* **84** 203
[64] Li E H 2000 *Semiconductor Quantum Well Intermixing—Material Properties and Optoelectronic Applications* (Amsterdam: Gordon and Breach)
[65] Kudrawiec R, Sek G, Rudno-Rudziński W, Misiewicz J, Wojcik J, Robinson B J, Thompson D A and Mascher P 2002 *Acta Phys. Pol.* A **102** 649
[66] Chan M C Y, Surya Ch and Wai P K 2001 *J. Appl. Phys.* **90** 197
[67] Kudrawiec R, Sek G, Misiewicz J, Li L H and Harmand J C 2003 *Appl. Phys. Lett.* **83** 1379
[68] Kudrawiec R, Misiewicz J, Fischer M and Forchel A 2004 *Phys. Status Solidi* a **201** 364
[69] Jezierski K, Markiewicz P, Misiewicz J, Panek M, Sciana B, Korbutowicz R and Tłaczała M 1995 *J. Appl. Phys.* **77** 4139